DYNAMIC WETTING OF AN OCCLUSION

Hossein Rashidian and Mathieu Sellier*

Mechanical Engineering Department,Unibversity of Canterbury,Christchurch8041,New Zealand

Philippe Mandin

Université de Bretagne Sud, IRDL, CNRS FRE 3744

*Address all correspondence to: Mathieu Sellier, E-mail: mathieu.sellier@canterbury.ac.nz

ABSTRACT

This paper investigates how and under which conditions the lamella of an impacting droplet is punctured by the presence of a small occlusion. Better understanding the conditions which lead to the rupture of the lamella is critical to produce defect free coating layers in the context of spray coating, for example. An analytical model based on surface energy analysis is proposed to obtain the critical thickness below which the liquid layer above the occlusion is unstable and lamella rupture occurs. Furthermore, we have developed a three dimensional multiphase lattice Boltzmann code to confirm the surface energy analysis and study the influence of key parameters like size of the occlusion, impact velocity and wettability of substrate on hole formation. Results show that a hole is more likely to appear as the diameter of the occlusion, the impact velocity, and the hydrophobicity of the surface increase.

KEY WORDS: Droplet impact, surface texture, hole formation, surface energy analysis, lattice Boltzmann method

1. INTRODUCTION

Many industrial applications involve the impact of a droplet on a substrates. Examples include spray painting and coating, food, agriculture, inject printing and spray cooling (Yarin, 2006; Andrade et al., 2013; Massinon and Lebeau, 2012; Castrejón-Pita et al., 2008 and Kim, 2007). Recently, Josserand and Thoroddsen (2015) have conducted an exhaustive review of the research related to the dynamics of wetting after impact on smooth and rough surfaces. Better understanding how the droplet wets the solid surface after impact is critical to obtain a better control in practical applications. For example, one may wish to avoid lamella break-up and the production of satellite droplets post-impact in the application of pesticide on foliage. Much is known about the wetting of a smooth surface. How surface texture affects this wetting is much less understood. Notwithstanding the fact that simple models are crucial to understand how the wetting front interacts with topographic features, only a few studies are available regarding droplet impact on smooth surfaces with isolated topographies (Josserand et al., 2005; de Jong

et al., 2015; Ellis et al., 2011; Sellier, 2015). For example; Josserand et al. (2005) studied experimentally and numerically the impact of a droplet on a substrate which features a single step topography and revealed that the step triggers a splash. de Jong et al. (2015) experimentally observed three various wetting outcomes including splash, air bubble and jet for a droplet impact close a millimetre-sized pit and two different wetting outcomes containing splash or no splash for a droplet impact close to a millimetre-sized pore. Ellis et al. (2011) compared the spreading rate computed analytically and numerically of a droplet impacting on various rough surfaces featuring a single step, a double-step, a two-sided steps and a periodic structure. Sellier (2015) investigated numerically how the contact line of a liquid film draining down on a vertical surface is influenced by an occlusion.

Hole formation in a thin sheet of liquid has fascinated many researchers in recent decades (Paddy, 1970; Taylor and Michael, 1973; Redon et al., 1991; Kheshgi and Scriven, 1991; Moriarty and Schwartz, 1993; Lopez et al., 2001; Bankoff et al., 2003 and Sellier et al., 2015). This dry spot which may lead to a rupture in a liquid film can be observed as the thickness of thin liquid film is decreased to a given threshold (Sharma and Ruckenstein, 1989). In the context of coating applications, the formation of hole in the lamella is considered a defect and therefore undesirable. Experiments have shown that the thin liquid film which is generated by a droplet impacting on a solid surface with an intermediate contact angle (around 100°) ruptures for a range of impact velocities, while the film rupture only occurs for the highest impact velocity when the substrate is either hydrophilic or super-hydrophobic (Dhiman and Chandra, 2010).

In spite of its obvious practical relevance, the problem of the wetting of a small occlusion by the lamella resulting from a droplet impact has not to date been investigated in a rigorous and systematic way. The goal of this study is to investigate how the presence of an occlusion can create a hole in the lamella of an impacting droplet. Once the contact line passes over the occlusion, the lamella thickness reduces to a minimum at maximum spread, thus a hole may form into the lamella on top of the occlusion as the thickness of the lamella becomes smaller than a critical film thickness. It can be anticipated that this critical film thickness is dependent on several parameters such as the impact velocity, the surface properties and the size of occlusion. We propose here an analytical model using surface energy analysis to demonstrate this hypothesis which we prove using numerical simulations.

To provide a greater understanding of the relation between hole formation in the lamella with the control parameters, the multiphase lattice Boltzmann method (LBM), a popular

mesoscopic numerical method, is implemented in this study. We have developed a three-dimensional multiphase lattice Boltzmann code following the Shan-Chen model (Shan and Chen, 1994) to simulate the behaviour of the lamella in the presence of the occlusion. Moreover, the centre of gravity of the droplet is tracked in our simulations to quantify the impact dynamics.

The remainder of the paper is structured as follows. Section 2 describes the multiphase lattice Boltzmann method in details. Then, we describe in section 3 the problem and propose the analytical surface energy model. As a validation case, we compare the thickness of the lamella at maximum spread which can be calculated through mass and momentum balance to our simulations as a crucial parameter in this study. Moreover, we present our numerical results and discuss the effects of control parameters on the dynamic wetting in this section. Finally, section 4 presents concluding remarks.

2. COMPUTATIONAL ALGORITHM

In the multiphase lattice Boltzmann method, a complex flow is modelled on a solution domain which is divided into lattices. Each lattice is occupied by either a fluid (liquid or gas) node or a solid node. For fluid nodes, an initial velocity u_0 needs to be assigned as well as an initial density ρ_0 which is either the gas density ρ_g and the liquid density ρ_l. To obtain the interaction between the fluids and the solid, the solid nodes possess an artificial wall density ρ_w where $\rho_g \leq \rho_w \leq \rho_l$ (Benzi et al., 2006). In fact, with the aid of the parameter ρ_w, different wall properties can be achieved and as a consequence various contact angles as demonstrated in (Rashidian and Sellier, 2017).

Discrete velocities models which play an essential role in the lattice Boltzmann method are specified as DnQm, where n denotes the space dimension and m denotes the number of velocities. The typical D3Q19 lattice arrangement is implemented in this study. This velocity model involves nineteen microscopic velocity vectors $\boldsymbol{e}_k$ in three space dimensions. The directions, k, are numbered like k = 0, 1,…, 18 and correspond to $\boldsymbol{e}_k$. For this velocity model, all the variables which need to be initialized are given as following:

$$[\boldsymbol{e}_0, \boldsymbol{e}_1, \boldsymbol{e}_2, \boldsymbol{e}_3, \boldsymbol{e}_4, \boldsymbol{e}_5, \boldsymbol{e}_6, \boldsymbol{e}_7, \boldsymbol{e}_8, \boldsymbol{e}_9, \boldsymbol{e}_{10}, \boldsymbol{e}_{11}, \boldsymbol{e}_{12}, \boldsymbol{e}_{13}, \boldsymbol{e}_{14}, \boldsymbol{e}_{15}, \boldsymbol{e}_{16}, \boldsymbol{e}_{17}, \boldsymbol{e}_{18}] \tag{1}$$

$$= c \begin{bmatrix} 0 & 1 & -1 & 0 & 0 & 0 & 0 & 1 & -1 & 1 & -1 & 1 & -1 & 1 & -1 & 0 & 0 & 0 & 0 \\ 0 & 0 & 0 & 1 & -1 & 0 & 0 & 1 & 1 & -1 & -1 & 0 & 0 & 0 & 0 & 1 & -1 & 1 & -1 \\ 0 & 0 & 0 & 0 & 0 & 1 & -1 & 0 & 0 & 0 & 0 & 1 & 1 & -1 & -1 & 1 & 1 & -1 & -1 \end{bmatrix}$$

In the above, c denotes the lattice speed which is given by $c = \frac{\Delta x}{\Delta t}$ where Δx and Δt are the lattice unit (lu) and the time step (ts), respectively. Furthermore, the sound speed is determined as $c_s^2 = \frac{c^2}{3}$ and the lattice weights are given by:

$$\omega_k = \begin{cases} 1/3 & k = 0 \\ 1/18 & k = 1,2,\dots,6 \\ 1/36 & k = 7,8,\dots,18 \end{cases} \quad (2)$$

The kinematic viscosity which is related to the relaxation time is defined as:

$$\upsilon = c_s^2(\tau - 0.5)\Delta t \quad (3)$$

where τ denotes the relaxation time and is adjusted to 1.

The main variable in the lattice Boltzmann method is the density distribution function $f_k(\boldsymbol{x}, t)$ which represents the state of a fluid parcel. A fraction of the distribution propagates with the lattice velocities $\boldsymbol{e_k}$ from a lattice position $\boldsymbol{x}$ to its neighbouring lattice $\boldsymbol{x} + \boldsymbol{e}_k \Delta t$ via certain directions or lattice links k at the following time step Δt. This process is called the streaming step and can be expressed by:

$$f_k(\boldsymbol{x} + \boldsymbol{e_k}\Delta t, t + \Delta t) = f_k(\boldsymbol{x}, t + \Delta t) \quad (4)$$

Note that for the lateral sides of the bounding box, periodic boundary conditions are applied for which the distribution functions carry on the opposite wall once they reach the end of the region.

On the other hand, a portion of other particles is moving from various directions to the same lattice simultaneously and therefore the collision step will take place at this lattice. The collision process which affects the numbers of original particles in each direction can be simplified to the Bhathagar-Gross-Krook (BGK) single relaxation time approximation (Bhathagar, Gross and Krook, 1954):

$$f_k(\boldsymbol{x}, t + \Delta t) = f_k(\boldsymbol{x}, t) + \frac{1}{\tau}(f_k^{eq}(\boldsymbol{x}, t) - f_k(\boldsymbol{x}, t)) \quad (5)$$

where f_k^{eq} denotes the equilibrium distribution function. To solve the above equation, the equilibrium distribution function needs to be calculated as:

$$f_k^{eq} = \omega_k \rho[1 + \frac{\boldsymbol{e_k}.\boldsymbol{u}}{c_s^2} + \frac{1}{2}\left(\frac{\boldsymbol{e_k}.\boldsymbol{u}}{c_s^2}\right)^2 - \frac{\boldsymbol{u}.\boldsymbol{u}}{2c_s^2}] \quad (6)$$

where ρ and $\boldsymbol{u}$ denote the fluid density and velocity, respectively. The following initial assumption can be applied as the relaxation time is unity:

$$f_k(\boldsymbol{x}, t = 0) = f_k^{eq}(\boldsymbol{x}, t = 0) = f_k^{eq}(\rho_0, \boldsymbol{u}_0) \quad (7)$$

In the collision step, we also consider bounce-back boundary conditions at the solid-liquid interface as the known distribution functions from the streaming process hit the wall and scatter back to the fluid via its incoming lattice link.

To calculate the equilibrium distribution function, we first need to obtain the macroscopic quantities from the density distributions. Accordingly,

$$\rho = \sum_{k=0}^{18} f_k \tag{8}$$

$$\boldsymbol{u} = \frac{1}{\rho} \sum_{k=0}^{18} f_k \, \boldsymbol{e}_k \tag{9}$$

The centre of gravity is determined according to:

$$\overline{\boldsymbol{z}} = \frac{\sum \boldsymbol{z_0}(\rho - \rho_g)}{\sum(\rho - \rho_g)} \tag{10}$$

where $\overline{\boldsymbol{z}}$ is the centre of gravity and $\boldsymbol{z_0}$ denotes the distance from the origin.

Shan and Chen (1994) introduced an alternative velocity named the equilibrium velocity for calculating the equilibrium distribution function:

$$\boldsymbol{u}^{eq} = \boldsymbol{u} + \frac{\boldsymbol{F}\,\tau}{\rho} \tag{11}$$

where $\boldsymbol{u}^{eq}$ replaces $\boldsymbol{u}$ in the equilibrium distribution function equation. $\boldsymbol{F}$ denotes the inter-particle force which can be obtained as:

$$\boldsymbol{F}(\boldsymbol{x}, t) = -G\psi(\boldsymbol{x}, t) \sum_{k=1}^{18} \omega_k \psi(\boldsymbol{x} + \boldsymbol{e_k}\Delta t, t)\boldsymbol{e_k} \tag{12}$$

where G denotes the strength controlling parameter and creates the liquid-gas interface with constant surface tension, density gradient and interface thickness. ψ denotes an pseudopotential term and is a function of density such that (Yuan and Schafer, 2006):

$$\psi(\rho) = \sqrt{\frac{2(P - c_s^2 \rho)}{6G}} \tag{13}$$

where P denotes the pressure and is determined from the following equation of state for a non-ideal fluid which makes a liquid-gas separation possible:

$$P = \rho\gamma T \frac{1 + \frac{\beta\rho}{4} + (\frac{\beta\rho}{4})^2 - (\frac{\beta\rho}{4})^3}{(1 - \frac{\beta\rho}{4})^3} - \alpha\rho^2 \tag{14}$$

According to Yuan and Schafer (2006) and Huang et al. (2011), T which denotes the temperature can be obtained by $T = 0.0943T_0$ as α =1 $lu^5/(mu.ts^2)$, β =4 lu^3/mu and γ =1 $lu^2/(ts^2 . tu)$. Note that mu and tu are the mass unit and the temperature unit, respectively.

After collision, a new collection of density distribution functions can leave this collision lattice and another streaming step starts. These steps are performed until a final desired time is reached. Finally, the density contours can be plotted to show the liquid behaviour during its interaction with the gas and the solid. The computational algorithm is summarized in Figure 1. In our simulation, the effect of gravity is neglected as it is assumed to be negligible compared to inertia and surface tension.

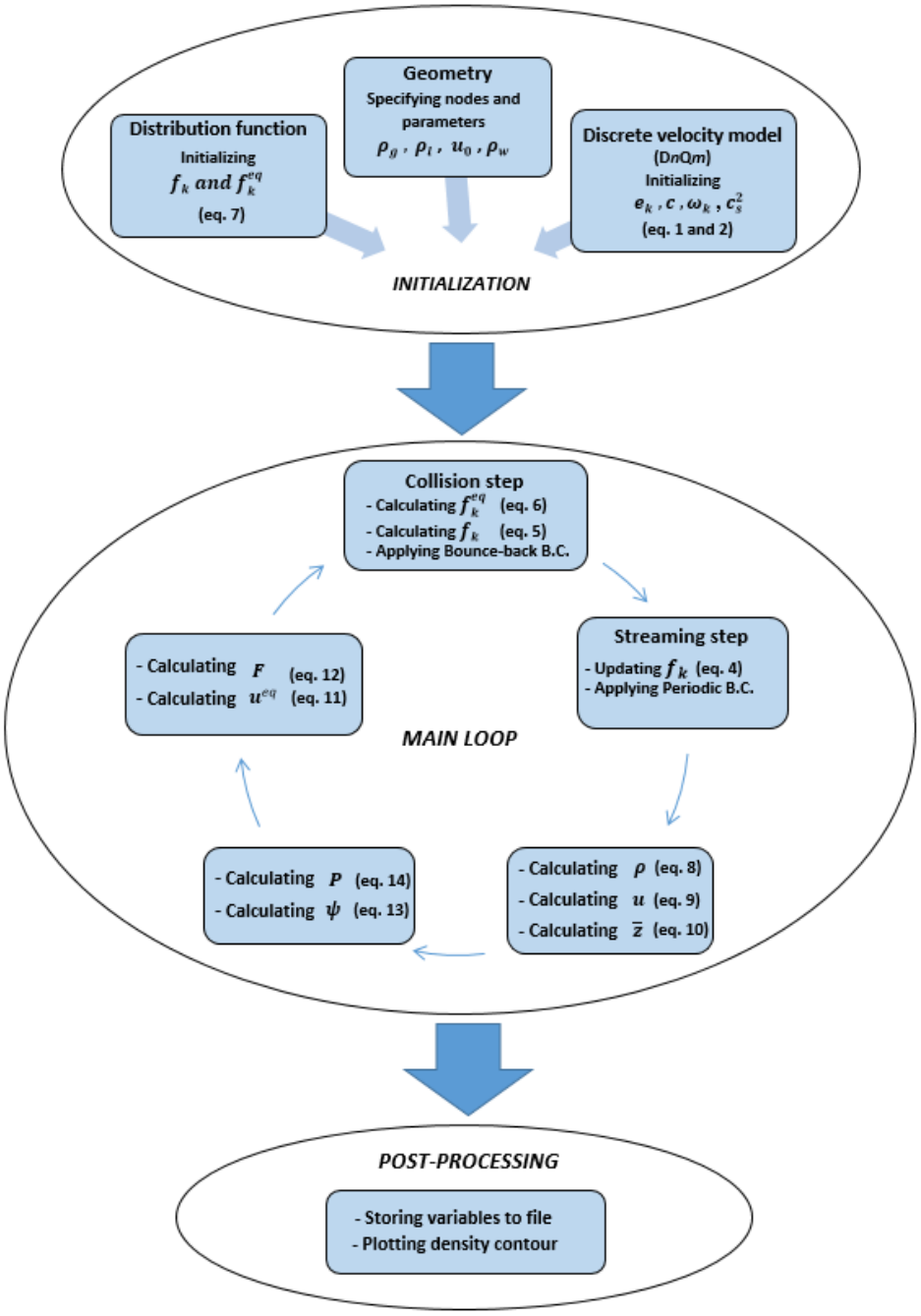

Figure 1. Schematic of the computational algorithm. This algorithm which has been developed following the Shan-Chen model consists of three main parts: firstly initialising variables and nodes, secondly a main loop involving the collision step, the streaming step, applying boundary conditions, calculating macroscopic quantities and the centre of gravity, determining pressure, pseudopotential term and forces and then obtaining the equilibrium velocity to update distribution functions in the next loop and finally a post-processing stage including plotting the density contours.

3. RESULTS AND DISCUSSION

Here we consider a spherical droplet which is initially located at the centre of a domain with size $L_x \times L_y \times L_Z = 260\ (lu) \times 260\ (lu) \times 90\ (lu)$. The droplet impacts and spreads onto a substrate which features a cylinder-shape occlusion as illustrated in Figure 2. The diameter of the droplet is $D = 65\ lu$ and the liquid and gas density are set to $\rho_l = 0.285\ (^{mu}/_{lu^3})$ and $\rho_g = 0.0285\ (^{mu}/_{lu^3})$, respectively. The distance from the impact point to the centre of the occlusion is kept constant ($L = 53\ lu$) and the size of the occlusion including the height (H) and the radius (r) are varied. During spreading, the lamella touches the occlusion and extends beyond it. At maximum spread, the occlusion may create a hole into the liquid film. We will show in the following that when the thickness of the liquid film on top of the occlusion is gradually reduced to reach a critical thickness (h_c), a hole is likely to form in the lamella (see Figure 3).

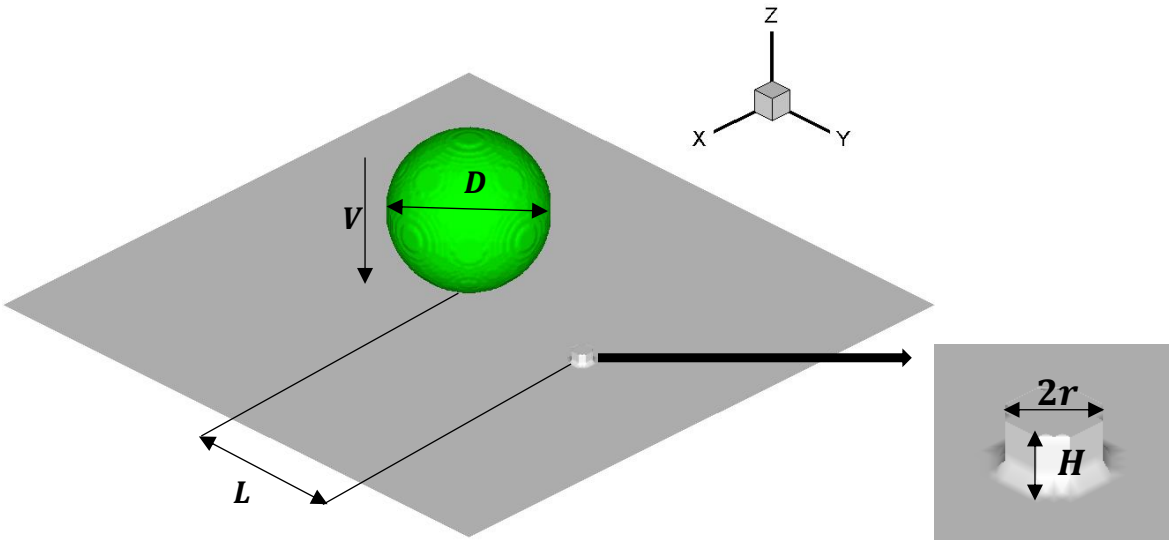

Figure 2. Simulation domain. A spherical droplet with a given diameter $D = 65$ and an initial velocity V impacts and spreads onto a substrate with a cylinder-shape occlusion with diameter $2r$ and height H . The distance from the impact point to the centre of the occlusion is $L = 53$ lu.

To obtain the critical thickness below which hole is likely to appear in the liquid film, a surface energy analysis is presented for both the lamella and the hole following Sharma and Ruckenstein (1989). Several assumptions are taken into account to simplify the analysis: the size of droplet, impact velocity and liquid properties are constant. Furthermore, the shape of the hole is a cylinder with a diameter equivalent to $2r$. Thus, the surface energy of the lamella becomes:

$$E_{lamella} = \gamma_{lg} A + \gamma_{sl} A' \tag{15}$$

where γ_{sl} and γ_{lg} denote the interfacial tension between solid-liquid and liquid-gas respectively. A is the surface area at the lamella-air interfaces and A' represents the surface area between the lamella and the substrate.

Now, when a hole is present on top of the occlusion, the surface energy is given by:

$$E_{hole} = \gamma_{lg}(A - \pi r^2) + \gamma_{sl}(A' - \pi r^2) + \gamma_{lg} 2\pi r h + \gamma_{sg}\pi r^2 \quad (16)$$

The total change in the surface energy is therefore given by:

$$\Delta E = E_{hole} - E_{lamella} = \pi r^2(-\gamma_{lg} - \gamma_{sl} + \gamma_{sg}) + 2\pi r h \gamma_{lg} \quad (17)$$

At this stage, we can substitute Young's equation (Quéré, 2008) which is $\gamma_{sg} - \gamma_{sl} = \gamma_{lg}\cos\theta$ into Equation 17 and therefore:

$$\Delta E = \gamma_{lg}(-\pi r^2 + \pi r^2 \cos\theta + 2\pi r h) \quad (18)$$

During retraction, if $\Delta E < 0$ then the hole grows in the lamella to break up around the occlusion and if $\Delta E > 0$ then the hole closes spontaneously. When $\Delta E = 0$, the critical thickness of the lamella on top of the occlusion to create the hole can be determined:

$$h_c = \frac{r(1-\cos\theta)}{2} \quad (19)$$

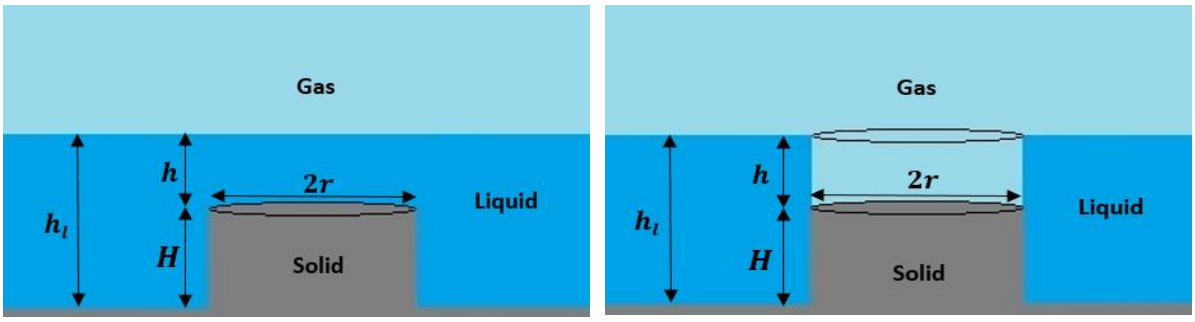

(a) (b)

Figure 3. At maximum spread, the thickness of the liquid film on top of the occlusion, h, is gradually decreased to reach a critical thickness, h_c,. (a) A hole is unlikely to exist as $h > h_c$ and (b) is likely to appear as $h < h_c$.

Consider a cylindrical shape for the lamella at maximum spread, the thickness of lamella at maximum spread (h_l) can be determined by a mass balance of the droplet before impact and at maximum spread:

$$h_l = \frac{2D}{3\xi^2} \quad (20)$$

where D is the diameter of the droplet before impact and ξ denotes the maximum spreading factor which is given by:

$$\xi = \frac{D_{max}}{D} \tag{21}$$

where D_{max} denotes the maximum spreading diameter. Scheller and Bousfield (1995) reported an empirical relationship based on the Reynolds and Weber numbers to obtain the maximum spreading factor:

$$\xi = 0.61\, Re^{1/5}\, (We\, Re^{-2/5}\,)^{1/6} \tag{22}$$

where the Reynolds and Weber numbers represent the ratio of inertia force to viscous and capillary forces, respectively. These dimensionless numbers are defined below:

$$Re = \frac{\rho_l V D}{\mu} \tag{23}$$

$$We = \frac{\rho_l V^2 D}{\sigma} \tag{24}$$

where σ denotes the surface tension of the liquid. Finally, the thickness of the lamella on top of the occlusion can be predicted as:

$$h = h_l - H \tag{25}$$

The centre of gravity of the droplet on the z-axis ($\overline{\boldsymbol{z}}$) during impact, spreading and retraction is computed during our lattice Boltzmann simulations of the droplet impact. This parameter can help us calculate the thickness of the lamella at maximum spread time. The centre of gravity for three different cases with various Reynolds and Weber numbers are plotted in Figure 4. Maximum spread occurs as the centre of gravity hits a minimum. The thickness of the lamella is assumed to be twice the distance between centre of gravity and the substrate. As a validation case, we compare the thickness of the lamella determined using the centre of gravity with the corresponding results when using the Scheller and Bousfield correlation (Equations 20-22). As Table 1 illustrated, a good agreement is found between the Lattice-Boltzmann simulation results and the correlation so that the error is less than 1%.

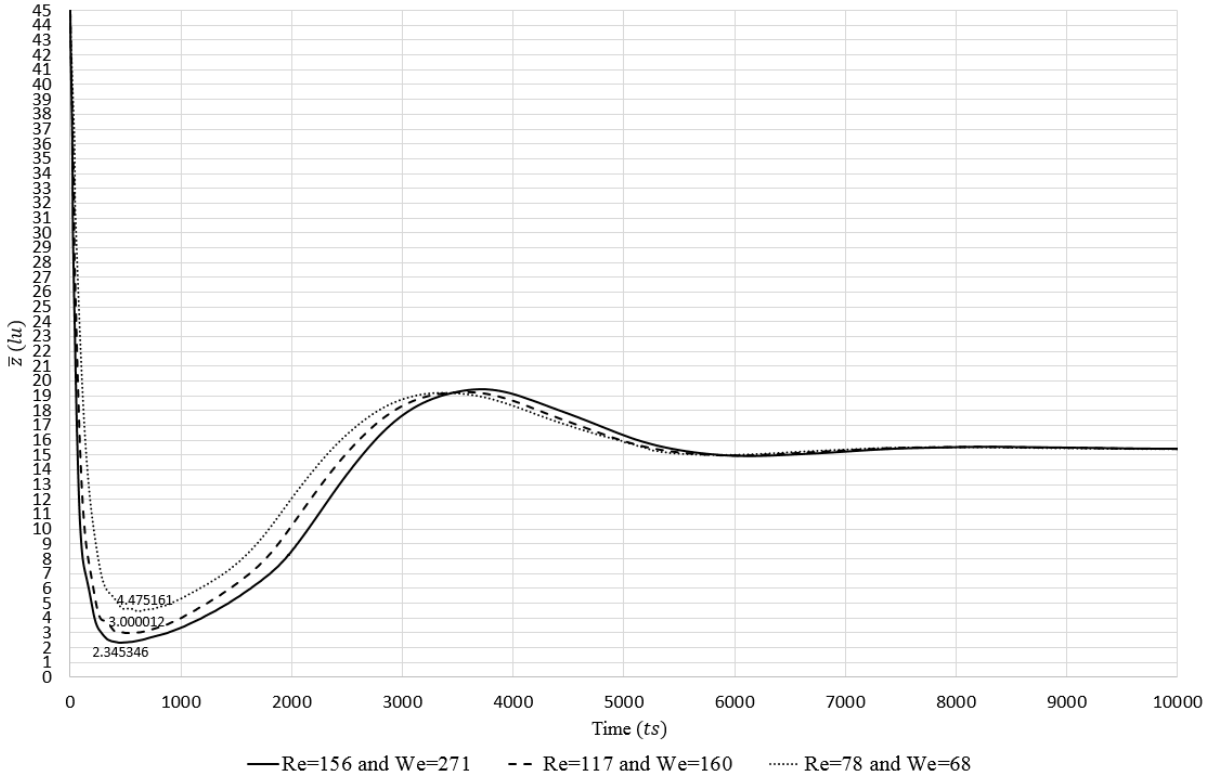

Figure 4. This plot demonstrates the location of the centre of gravity on the z-axis ($\overline{z}$) as the droplet falls, impacts, spreads and retracts on the substrate without occlusion. At maximum spread, the centre of gravity hits a minimum. The minimum amount of $\overline{z}$ shows for each graph. The thickness of the lamella is assumed to be twice this minimum.

Table 1. Comparision of the lamella thickness at maximum spread between Scheller and Bousfield correlation (using Equations 20-22) and the numerical solution (using centre of gravity in z-axis)

Re	***We***	**h_l analytical solution (lu)**	**h_l numerical solution (lu)**
78	68	8.92	8.95
117	160	6.02	6
156	271	4.68	4.69

3.1 Effect of the occlusion size

Equation 19 illustrates that an increase in the diameter of the occlusion leads to an increase of the thickness threshold. To demonstrate this expected correlation, several simulations are carried out for a constant height of the occlusion ($H = 5\ lu$) but varied diameters. The equilibrium contact angle is adjusted to $\theta = 90°$, the Reynolds and Weber number are set to 117 and 160, respectively. We will first consider $h_l = 6\ lu$ such that the thickness of lamella on top of the occlusion is 1 lu. For $r = 4\ lu$, once the lamella reaches maximum spread, a hole is created (as shown in Figure 5a) as the thickness of the liquid film on top of the occlusion ($h = 1\ lu$) is less than its critical thickness ($h_c = 2\ lu$). During retraction, the hole is growing

until a break-up occurs around the occlusion (Figure 5b) and then the droplet recoil to a steady state condition with a contact angle of 90°(Figure 5c).

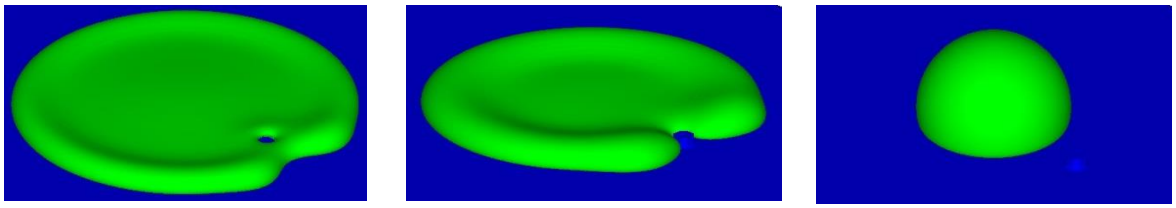

(a) (b) (c)

Figure 5. Simulation results for the first case as $r = 4\ lu$ and $\theta = 90°$. (a) The hole is created as $h < h_c$ at maximum spread of lamella: (b) During retraction a break-up occurs in the lamella around the occlusion. (c) The droplet steadies at the impact point with its equilibrium contact angle.

We consider next a set of conditions for which the thickness of the liquid film on top of the occlusion and the critical thickness are identical. Thus, for the second case, we consider $r = 2\ lu$ and consequently $h = h_c = 1\ lu$. The simulation results are depicted in Figure 6. It can be seen that a hole is created at maximum spread (figure 6a); however, this hole closes spontaneously during retraction since the film thickness on top of the occlusion becomes larger than the threshold value (Figure 6b). In fact, the surface energy of the lamella which was defeated by the surface energy of the hole at maximum spread ($\Delta E \leq 0$) overcomes the hole energy during retraction ($\Delta E > 0$) due to the thickness of liquid film on top of the occlusion exceeding the critical value $h_c = 1\ lu$. Therefore, the hole is unable to grow, the liquid film "heals" and eventually retraction occurs without break-up (figure 6c).

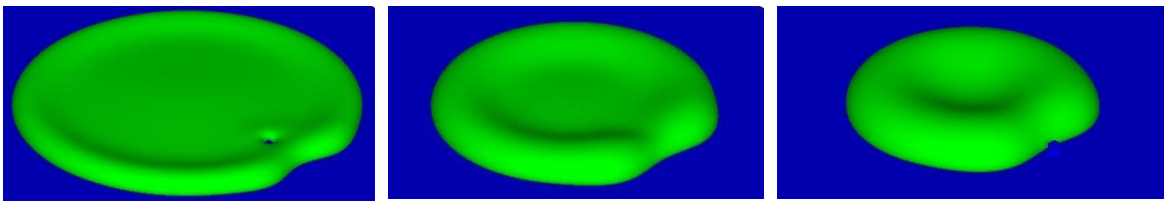

(a) (b) (c)

Figure 6. Simulation results for the second case as $r = 2\ lu$ and $\theta = 90°$. (a) At maximum spread of lamella: the thickness of lamella on top of the occlusion and the critical thickness ($h = h_c = 1lu$) and therefore hole is created. (b) But the hole closes spontaneously due to $h > h_c$ during retraction. (c) The lamella pass over the occlusion during retraction without break-up.

In the third case, H is reduced from 5 lu to 3 lu and other parameters are kept the same as case 1 to confirm that an increase in the thickness of the lamella on top of the occlusion by an amount greater than the critical thickness leads to the absence of hole generation during spreading and retraction. The simulation results demonstrate that a hole does not form for this

case during spreading and retraction because to $h > h_c$ (see Figure 7a). The results of this section are summarized in Table 2.

Table 2. Dynamic wetting status of the occlusion for three different cases with various sizes of the occlusion (r and H) as $\theta = 90°$, Re=117 and We=160. For these equilibrium contact angle, Reynolds and Weber numbers, the thickness of the lamella at maximum spread is $h_l = 6\ lu$ and therefore the thickness of the lamella on top of the occlusion (h) is determined using Equation 26. The critical thickness is calculated using Equation 20.

Case	$r\ (lu)$	$H\ (lu)$	$h\ (lu)$	$h_c\ (lu)$	status
1	4	5	1	2	Hole formation
2	2	5	1	1	Hole formation occurs only at maximum spread and then the hole closes during retraction
3	4	3	3	2	No hole formation

3.2 Effect of the impact velocity

In this section, two other cases are investigated to show the influence of the impact velocity on hole formation. Firstly, in case 3 of section 3.1 for which we did not observe any hole the impact velocity is increased until the Reynolds number and the Weber number becomes 156 and 271, respectively. As illustrated in Table 1, h_l is determined to be 4.7 lu from both the analytical solution and the numerical solution. According to Equation 27, the thickness of the lamella on top of the occlusion yields $h = 1.7\ lu$. As shown in Figure 7b, a hole is observed for that case because h is now smaller than h_c at maximum spread .The increase in the impact velocity leads to a smaller lamella thickness and the likely appearance of a hole as intuitively expected. Secondly, in the case 1 of section 3.1 for which we did observe the formation of a hole, the impact velocity is reduced until the Reynolds and Weber numbers becomes 100 and 111, respectively and therefore h_l is calculated to be 7.9 lu. In this case, h is larger than its threshold and thus no hole is created as confirmed by Figure 7c.

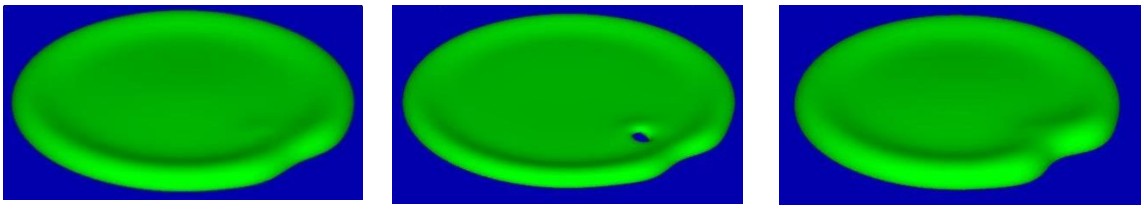

(a) (b) (c)

Figure 7. Simulation results (a) the hole is not created as $r = 4\ lu$ and $H = 3\ lu$ (Re=117 and We=160) due to $h > h_c$. (b) With increase the impact velocity (Re =156 and We =271) the hole forms on top of the occlusion due to $h < h_c$. (c) In this case the Reynolds and Weber numbers of the case 1 in section 4.1 ($r = 4\ lu$ and $H = 5\ lu$) are decreased to Re =100 and We =111 and therefore the hole is not created due to $h > h_c$.

3.3 Effect of the substrate wettability

In this section, the diameter of the occlusion is kept constant and θ is varied to investigate the influence of the substrate wettability on hole formation. As Equation 19 shows, the critical thickness reduces with increased wettability of the surface and vice-versa. The critical film thickness h_c for hydrophobic surfaces is larger than h_c for hydrophilic surfaces and thus hole formation is more likely to occur for increasing hydrophobicity. The simulation results also confirm this correlation. For instance; for a same parameters as those of case 3 in section 4.1, when θ increases from 90° to 135°, the critical thickness becomes 3.4 lu and therefore hole formation occurs during spreading because $h < h_c$, while no hole formed when $\theta = 90°$. Figure 8 shows the simulations for $\theta = 135°$ and it can be seen that a hole is created at maximum spread time (Figure 8a). The hole then grows towards the centre of liquid film during retraction and a break-up occurs around the occlusion (Figure 8b). Finally the droplet recoils to a spherical cap configuration centered at the impact point with its equilibrium contact angle (Figure 8c).

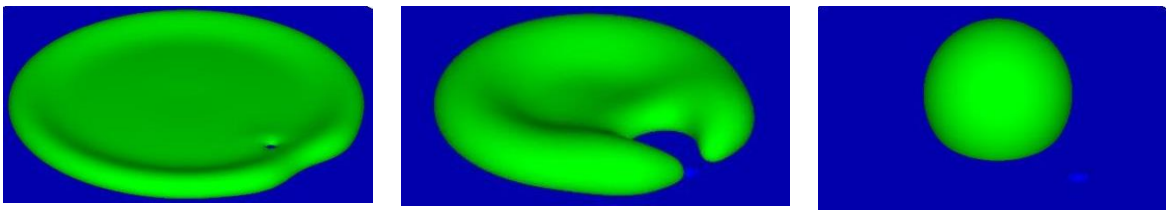

(a) (b) (c)

Figure 8. Simulation results (a) In case 3 of section 4.1 ($r = 4$ lu and $H = 3$ lu), with increasing the equilibrium contact angle of the substrate from $\theta = 90°$ to $\theta = 135°$, a hole forms on top of the occlusion because $h < h_c$. (b) During retraction, the lamella around the occlusion breaks up (see the size of the hole once the break-up occurs). (c) Finally, the droplet sits at the impact point with equilibrium contact angle of 135°.

Moreover, we carried out another simulation for which all parameters are the same as case 1 in section 4.1 and only θ is reduced from 90° to 45°. For $\theta = 90°$ we observed that the hole was created, whereas for $\theta = 45°$ no hole is observed (see Figures 9a) and as a consequence further confirm that a hole is unlikely to appear as surface wettability increased. It also interesting to note that when the surface wettability is enhanced, the droplet likes to adhere to the occlusion during retraction (Figure 9b). Thus, the droplet centre of gravity moves from the impact point to a new location closer to the occlusion and adheres to it at its equilibrium contact angle (Figure 9c).

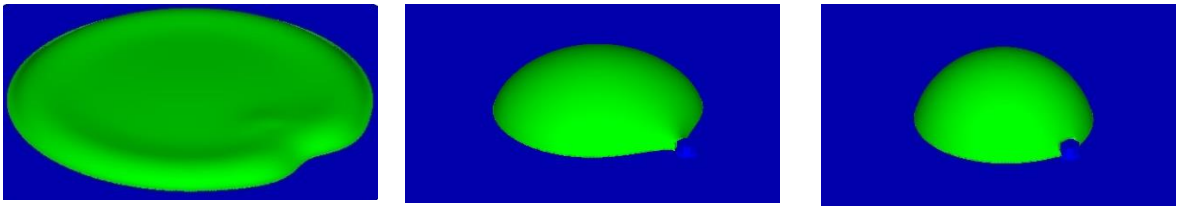

(a) (b) (c)

Figure 9. Simulation results (a) In case 1 of section 4.1 ($r = 4\ lu$ and $H = 5lu$), no hole can be observed as the wettability of the substrate decreases from $\theta = 90°$ to $\theta = 135°$. (b) During retraction, the droplet sticks to the occlusion (c) The droplet moves from the impact point to the occlusion position and sits alongside of the occlusion at its equilibrium contact angle.

4. CONCLUSION

In this study, we have performed a surface energy analysis and numerical simulations to investigate how an occlusion may form a hole into the liquid film which is generated by an impacting droplet. This hole formation has been observed as the thickness of the liquid film on top of the occlusion (h) is reduced to reach a critical thickness (h_c). Based on our analytical investigation which involves several simplifying assumption, this critical film thickness depends on the diameter of the occlusion and the wettability of the substrate. Furthermore, the impact velocity plays an essential role on hole formation because the thickness of the lamella (h_l) is reduced when the impact velocity increases. This reduction in h_l leads to a decrease h to a value smaller than h_c and therefore a hole is likely to appear in the lamella.

To confirm these expected trends, we have developed a multiphase lattice Boltzmann code in three-dimensional space following the Shan-Chen model. In our code, h_l at maximum spread was assumed to be twice the distance between the centre of gravity and the substrate. As a validation case, we compared the numerical results for h_l with the corresponding correlation of Scheller and Bousfield (1995). The results showed a very good agreement hence confirming the correct implementation of the algorithm. Then, the effect of various control parameters on hole formation was investigated numerically. The numerical simulations demonstrated that the hole is more likely to form as the diameter of the occlusion, the impact velocity and hydrophobicity of the substrate increase, as one would expect. It has been also observed that with increasing the wettability of substrate, the droplet endeavour to stick to the occlusion during retraction opening up interesting opportunity to control droplets on surfaces after impact

5. REFERENCES

Andrade, R., Skurtys, O., Osorio, F., 2013. Drop impact behaviour on food using spray coating: fundamentals and applications. Food research international, 54(1), 397-405.

Bankoff, S. G., Johnson, M. F. G., Miksis, M. J., Schluter, R. A., Lopez, P. G., 2003. Dynamics of a dry spot. Journal of Fluid Mechanics, 486, 239-259.

Benzi, R., Biferale, L., Sbragaglia, M., Succi, S., Toschi, F., 2006. Mesoscopic modelling of a two-phase flow in the presence of boundaries: the contact angle. Physical Review E, 74(2), 021509.

Bhatnagar, P.L., Gross, E.P., Krook, M., 1954. A model for collision processes in gases. I. Small amplitude processes in charged and neutral one-component systems. Physical review, 94(3), 511.

Castrejón-Pita, J.R., Martin, G.D., Hoath, S.D., Hutchings, I.M., 2008. A simple large-scale droplet generator for studies of inkjet printing. Review of Scientific Instruments, 79(7), 075108.

de Jong, R., Enríquez, O.R., van der Meer, D., 2015. Exploring droplet impact near a millimetre-sized hole: comparing a closed pit with an open-ended pore. Journal of fluid mechanics, 772, 427-444.

Dhiman, R., Chandra, S., 2010. April. Rupture of thin films formed during droplet impact. In Proceedings of the Royal Society of London A: Mathematical, Physical and Engineering Sciences, 466(2116), 1229-1245.

Ellis, A.S., Smith, F.T., White, A.H., 2011. Droplet impact on to a rough surface. Quarterly Journal of Mechanics & Applied Mathematics, 64(2).

Huang, H., Krafczyk, M., Lu, X., 2011. Forcing term in single-phase and Shan-Chen-type multiphase lattice Boltzmann models. Physical Review E, 84(4), 046710.

Hyväluoma, J., Harting, J., 2008. Slip flow over structured surfaces with entrapped microbubbles. Physical review letters, 100(24), 246001.

Josserand, C., Lemoyne, L., Troeger, R., Zaleski, S., 2005. Droplet impact on a dry surface: triggering the splash with a small obstacle. Journal of fluid mechanics, 524, 47-56.

Josserand, C. and Thoroddsen, S.T., 2016. Drop impact on a solid surface. Annual Review of Fluid Mechanics, 48, 365-391.

Kheshgi, H.S., Scriven, L.E., 1991. Dewetting: Nucleation and growth of dry regions. Chemical engineering science, 46(2), 519-526.

Kim, J., 2007. Spray cooling heat transfer: the state of the art. International Journal of Heat and Fluid Flow, 28(4), 753-767.

López, P. G., Miksis, M. J., Bankoff, S. G., 2001. Stability and evolution of a dry spot. Physics of Fluids, 13(6), 1601-1614.

Massinon, M., Lebeau, F., 2012. Experimental method for the assessment of agricultural spray retention based on high-speed imaging of drop impact on a synthetic superhydrophobic surface. Biosystems Engineering, 112(1), 56-64.

Mohamad, A.A., 2011. Lattice Boltzmann method: fundamentals and engineering applications with computer codes. Springer Science & Business Media.

Moriarty, J. A., Schwartz, L. W., 1993. Dynamic considerations in the closing and opening of holes in thin liquid films. Journal of colloid and interface science, 161(2), 335-342.

Padday, J.F., 1970. Cohesive properties of thin films of liquids adhering to a solid surface. Special Discussions of the Faraday Society, 1, 64-74.

Quéré, D., 2008. Wetting and roughness. Annu. Rev. Mater. Res., 38, 71-99.

Rashidian H., Sellier, M., 2017, Modelling an impact droplet on a pair of pillars. Interfacial Phenomena and Heat Transfer, 5(1), 43-57.

Redon, C., Brochard-Wyart, F., Rondelez, F., 1991. Dynamics of dewetting. Physical review letters, 66(6), 715.

Scheller, B.L., Bousfield, D.W., 1995. Newtonian drop impact with a solid surface. AIChE Journal, 41(6), 1357-1367.

Sellier, M., 2015. Modelling the wetting of a solid occlusion by a liquid film. International Journal of Multiphase Flow, 71, 66-73.

Sellier, M., Grayson, J. W., Renbaum-Wolff, L., Song, M., Bertram, A. K., 2015. Estimating the viscosity of a highly viscous liquid droplet through the relaxation time of a dry spot. Journal of Rheology, 59(3), 733-750.

Shan, X., Chen, H., 1994. Simulation of nonideal gases and liquid-gas phase transitions by the Lattice Boltzmann equation. Physical Review E, 49(4), 2941.

Sharma, A., Ruckenstein, E., 1989. Dewetting of solids by the formation of holes in macroscopic liquid films. Journal of colloid and interface science, 133(2), 358-368.

Taylor, G.I., Michael, D.H., 1973. On making holes in a sheet of fluid. Journal of fluid mechanics, 58(4), 625-639.

Yarin, A.L., 2006. Drop impact dynamics: splashing, spreading, receding, bouncing…. Annu. Rev. Fluid Mech., 38, 159-192.

Yuan, P., Schaefer, L., 2006. Equations of state in a Lattice Boltzmann model. Physics of Fluids, 18(4), 042101.

Zu, Y.Q., Yan, Y.Y., 2016. Single droplet on micro square-post patterned surfaces–theoretical model and numerical simulation. Scientific reports, 6.